Food Chemistry 431 (2024) 137094

Contents lists available at ScienceDirect

Food Chemistry

journal homepage: www.elsevier.com/locate/foodchem

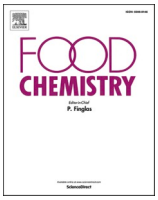

Movements of moisture and acid in gastric milk clots during gastric digestion: Spatiotemporal mapping using hyperspectral imaging

Siqi Li [a,1], Yash Dixit [b,1], Marlon M. Reis [b,*], Harjinder Singh [a], Aiqian Ye [a,*]

[a] Riddet Institute, Massey University, Private Bag 11 222, Palmerston North 4442, New Zealand
[b] AgResearch Ltd, Te Ohu Rangahau Kai, Private Bag 11 008, Palmerston North, New Zealand

ARTICLE INFO

Keywords:
Gastric digestion
Milk
Hyperspectral imaging
Gastric acid
Moisture transfer
Food structure

ABSTRACT

Ruminant milk is known to coagulate into structured clots during gastric digestion. This study investigated the movements of moisture and acid in skim milk clots formed during dynamic gastric digestion and the effects of milk type (regular or calcium-rich) and the presence/absence of pepsin. We conducted hyperspectral imaging analysis and successfully modelled the moisture contents based on the spectral information using partial least squares regression. We generated prediction maps of the spatiotemporal distribution of moisture within the samples at different stages of gastric digestion. Simultaneously to acid uptake, the moisture in the milk clots tended to decrease over the digestion time; this was significantly promoted by pepsin. Moisture mapping by hyperspectral imaging demonstrated that the high and low moisture zones were centralized within the clot and at the surface respectively. A structural compaction process promoted by pepsinolysis and acidification probably contributed to the water expulsion from the clots during digestion.

1. Introduction

The gastric digestion of food is a critical process that determines overall digestive dynamics and nutritional outcomes. Ingested food undergoes mechanical breakdown as well as chemical hydrolysis by the gastric secretions of enzymes and acid (Bornhorst & Singh, 2014). During gastric digestion, the movements of acid and moisture within the solid food chyme are important for the intragastric structural development and digestion kinetics of the ingested foods (Guo, Ye, Singh, & Rousseau, 2020). The intragastric pH can modulate the activity and specificity of pepsin (Mennah-Govela, Swackhamer, Bornhorst, 2021; Piper & Fenton, 1965; Yang et al., 2022) and the dissolution of minerals that are not fully soluble at the natural pH of the food (Choki, Li, Ye, Jameson, & Singh, 2021). Typically, moisture and acid migrate into the food structure from the surrounding gastric environment (Mennah-Govela & Bornhorst, 2016a, 2016b; Somaratne et al., 2019). However, previous studies have shown that the kinetics of acid and moisture uptake into food structures during gastric digestion do not always follow the same pattern, probably because of their different driving forces (Deng, Mars, van der Sman, Smeets, & Janssen, 2020; Mennah-Govela & Bornhorst, 2016b). Furthermore, whereas acid mostly transfers towards the inside of the food, water can move in both directions, from the gastric environment to the food and vice versa, e.g. the swelling and shrinking of protein gels (Deng et al., 2020; van der Sman, Houlder, Cornet, & Janssen, 2020).

Much research on modelling the kinetics of the transfer of moisture and acid in model foods during gastric digestion has been conducted (Mennah-Govela & Bornhorst, 2016a, 2016b; van der Sman et al., 2020). However, the spatial gradients within the food particles have often not been considered, and they could have a significant impact on the digestion process (Somaratne et al., 2019; van der Sman et al., 2020). Some studies have investigated the spatiotemporal distribution of moisture, acid and pepsin within food structures under gastric digestion conditions (Kong, Oztop, Singh, & McCarthy, 2013; Nau et al., 2022; Somaratne et al., 2019).

Hyperspectral imaging (HSI) is a non-invasive analytical technique that collects a spectrum per pixel in an area of interest. The use of HSI with spectra in the near-infrared spectral range allows the prediction of chemical composition for the corresponding pixel enabling the development of chemical maps (Reis et al.,2023). HSI has been used for the evaluation of food composition and quality, including the dynamic changes during the processing, storage and cooking of foods (Liu, Pu, &

* Corresponding author.
E-mail addresses: marlon.m.reis@agresearch.co.nz (M.M. Reis), a.m.ye@massey.ac.nz (A. Ye).
[1] These authors contributed equally to this work.

https://doi.org/10.1016/j.foodchem.2023.137094
Received 22 May 2023; Received in revised form 25 July 2023; Accepted 2 August 2023
Available online 6 August 2023

Sun, 2017). Zhu et al. (2016) utilized HSI to generate chemical maps for total acid content and moisture content during solid-state fermentation. Jiang et al. (2021) applied HSI to map the distribution of total acid content during the fermentation of Daqu. Somaratne et al. (2019) utilized HSI to characterize the spatiotemporal distributions of moisture and acid within food structures during the simulated gastric digestion of sweet potatoes and egg white gels. These successful applications show that HSI is a powerful new technique for understanding the digestion of food, during which complex physicochemical changes take place.

Among common foods, ruminant milk uniquely undergoes coagulation during gastric digestion and forms a coagulum that is commonly referred to as "clots" or "curds" (Huppertz & Chia, 2020; Li et al., 2022a; Ye, Cui, Dalgleish, & Singh, 2016). By investigating the digestion behaviour of milk with and without pepsin in a dynamic in vitro gastric digestion system, Ye et al. (2016) demonstrated that the coagulation of milk arises from the cleavage of κ-caseins at the casein micelle surface by pepsin during early gastric digestion, which destabilizes the casein micelles and results in their aggregation. The gastric coagulation of milk is affected by processing treatments (Li et al., 2022a; Li, Ye, & Singh, 2021; Ye et al., 2019), the presence of fat (Mulet-Cabero et al., 2020) and colloidal calcium phosphate (CCP) (Huppertz & Lambers, 2020). Interestingly, previous studies have reported that the moisture content of gastric milk clots decreases during the first 2 h of gastric digestion, both in vitro (Li et al., 2022a; Roy, Ye, Moughan, & Singh, 2021) and in vivo (Ye et al., 2019). This behaviour is unique, in the sense that water rarely moves from the solid structures of the food chyme to the surrounding gastric juice environment, against the direction of the concentration gradient. As the moisture content of the milk clots in the stomach has been found to be associated with their textural properties, which affect their breakdown during digestion (Li et al., 2022a), understanding the spatiotemporal distribution of moisture within the structure of milk clots, and its relationship with acid uptake during gastric digestion, will provide novel insights into the dynamic digestion process of milk and dairy foods. Furthermore, unlike protein gels, which are similar in chemical nature but will undergo mastication and size reduction before reaching the stomach (Deng et al., 2020; Somaratne et al., 2019), milk clots of considerable size form dynamically in the stomach (Li et al., 2022a; Roy et al., 2022). Thus, an understanding of the dynamic changes in the transfer of acid and moisture in milk clots will better reflect real-life scenarios.

This study investigated the dynamic movement and the distribution of moisture and acidity in skim milk clots during in vitro gastric digestion employing HSI. Given the previously reported moisture loss from milk clots during gastric digestion (Li et al., 2022a; Roy et al., 2021; Ye et al., 2019), we hypothesized that the patterns of movement of moisture and acid would be markedly different. The effects of the presence or absence of pepsin and two commercially available pasteurized skim milk types (different in calcium and protein contents) were investigated. Milk clots were prepared under established dynamic gastric digestion conditions, cut into cylinders of defined size and then incubated under static gastric digestion conditions for different periods, with and without pepsin. Then, chemical analyses to understand the bulk changes in the mass, acidity and moisture of the digested samples were conducted. The data along with the HSI spectra of the digested samples were fitted and modelled to generate prediction maps of spatiotemporal distributions.

2. Materials and methods

2.1. Materials

Two types of commercial pasteurized fat-free milk purchased from a local supermarket in Palmerston North, New Zealand, were studied: regular skim milk (SM) and calcium-rich skim milk (CaSM). The SM consisted of 4 g of protein, 0.1 g of fat, 5 g of lactose and 133 mg of calcium per 100 mL. The CaSM had higher calcium (190 mg/100 mL) and protein (5.8 g/100 mL) contents than the SM; they were hypothesized to affect the gastric coagulation and digestion behaviours (Huppertz & Lambers, 2020; Panthi, Kelly, O'Callaghan, & Sheehan, 2019). All chemicals were purchased from Sigma Aldrich (St. Louis, MO, USA.). Simulated salivary fluid and simulated gastric fluid (SGF) were prepared as described by Brodkorb et al. (2019).

2.2. Preparation of skim milk clots by dynamic in vitro gastric digestion

To standardise the dimensions of milk clot samples for further chemical and HSI analyses, we conducted gastric digestion experiments in two phases: a brief dynamic digestion step to obtain milk clots formed under dynamic gastric digestion conditions followed by a second step of static gastric digestion after cutting the milk clots into cylinders.

Gastric milk clots were prepared by a brief 20-min digestion process in a dynamic in vitro gastric digestion system, the human gastric simulator, as described previously (Li et al., 2022a; Ye et al., 2019). Briefly, 250 g of milk was warmed to 37 °C, mixed with 30 g of simulated salivary fluid and introduced into the human gastric simulator. A 20 mL aliquot of SGF (pH 1.5, pepsin activity 2000 U/mL) was added at the beginning of the digestion as the basal amount in a fasted state. Dynamic gastric digestion was performed at 37 °C for 20 min. SGF was gradually added during the digestion process at a rate of 2.5 mL/min. After 20 min of dynamic digestion, when the pH of the gastric liquid phase was around 5.8–6.0, an intact piece of milk clot had formed. The fresh clot was rinsed with reverse osmosis water to remove acid and pepsin at the surface.

2.3. Incubation of milk clots under static gastric digestion conditions

The preparation of milk clot samples for static gastric digestion was modified from Somaratne et al. (2019) and is illustrated in Fig. 1. Each milk clot was cut through the centre to obtain a cylinder of defined dimensions (3 cm long, 1.5 cm diameter). For this purpose, a sampling tool was crafted from a stainless steel pipe at a mechanical workshop (School of Food and Advanced Technology, Massey University), with one end sharpened for effective cutting and a plunger inside for pushing out the sample. Plastic caps of 1.5 cm internal diameter and 0.5 cm height were fixed onto both ends of the milk clot cylinders using a waterproof sealant. This was to limit the mass transfer to only the radial direction of the cylinders during incubation. For static digestion, each cylinder was placed in a container with 100 mL of SGF (pre-warmed to 37 °C, with pepsin at 2000 U/mL or without pepsin, pH 2.0). The clot samples were incubated separately for up to 220 min in a shaking incubator (50 rev/min, 37 °C). Clot cylinders incubated for 0, 20, 40, 100, 160 and 220 min were collected, quickly rinsed with deionized water to remove the digestion fluid and gently tapped with a tissue to remove water on the surface. Then, two slices of samples of 5 mm thickness were carefully cut out from the centre of the cylinder using a surgical blade and were placed in a petri dish for HSI and following physicochemical analyses (Fig. 1). Three independent experiments were performed for each milk type, the presence/absence of pepsin and each digestion time point.

2.4. Hyperspectral imaging system and image acquisition

Fig. 1 also presents a schematic diagram of the HSI system and the steps from image acquisition to prediction mapping. The hyperspectral system included a translation stage, an illumination system and a hyperspectral camera. The illumination system (Headwall Photonics, Fitchburg, MA, USA) consisted of one halogen lamp light source (JCR 21 V 150 W/AL Japan 2DB) and was designed to distribute the light uniformly over the line detected by the camera. The power of the light source was adjusted using a white reference tile. The highest intensity detected in the white reference tile was set as 85% saturation of the detector. This was done to prevent detector saturation in certain regions of the sample, which could produce a specular reflection. The same white tile was used for all scanning, ensuring consistency of the scanning

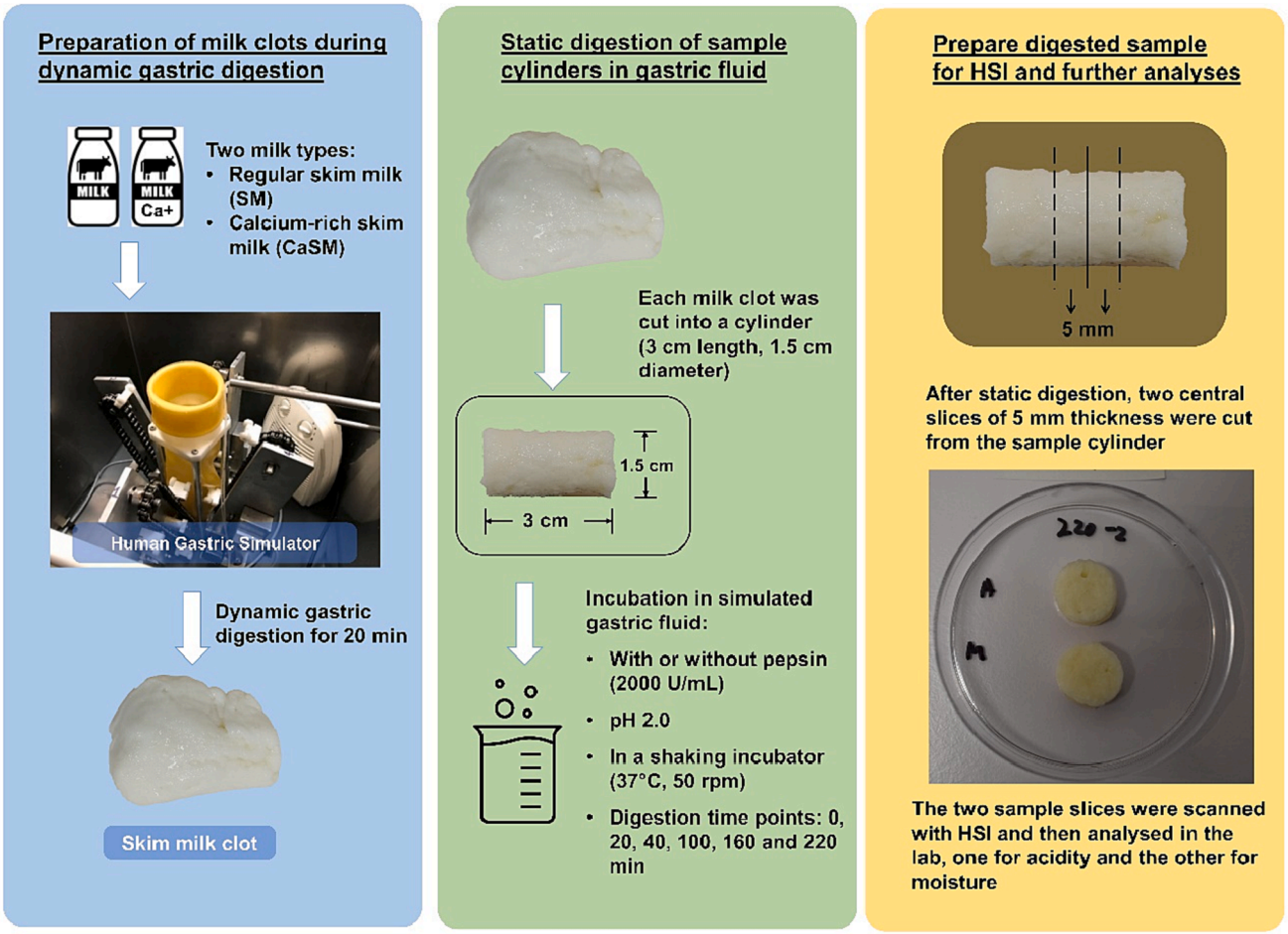

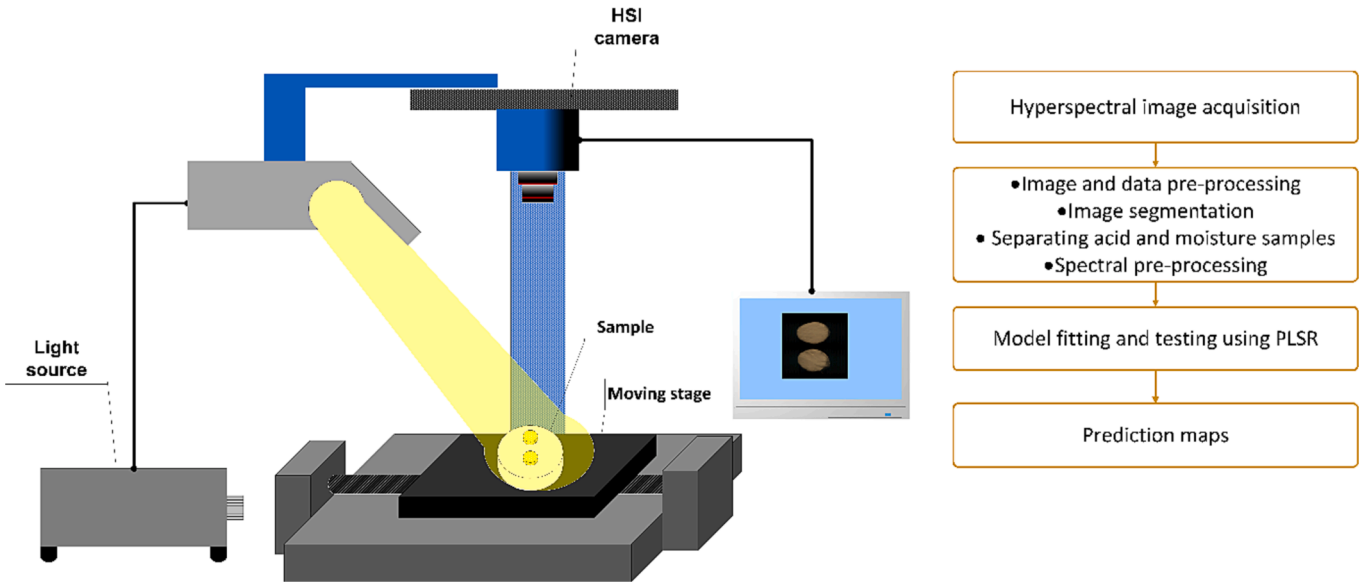

Fig. 1. Schematic diagrams of in vitro digestion and preparation of skim milk clot samples before hyperspectral imaging (HSI) and chemical analysis (top) and the HSI system and the steps from image acquisition to prediction mapping (bottom). PLSR, partial least squares regression.

condition. The translation stage included a motorized system (VT-80 linear translation stage/PI micos with DC controller/driver DC-Mcco/PI micos). The hyperspectral camera included a Headwall spectrograph (Model 1003B-10151; Headwall Photonics) that captured 320 spectra in a line. Each spectrum had 235 wavelengths in the spectral range 550–1700 nm with a spectral resolution of 5 nm. The exposure time used (39 ms), the frame period (50 ms) and the linear translation speed (4.8 mm/s) were adjusted to ensure that the pixels were square with a spatial resolution of about 0.4 mm × 0.4 mm for one pixel. A 35 mm lens (67716 VIS-NIR, Edmund Optics) with an aperture of f/2.8 was utilized. This aperture was chosen to ensure the field view of the lens described the thickness of samples and described variation caused by uneven

surfaces on the samples. The distance between the sample and the lens was 220 mm. All images were calibrated to obtain the reflectance values as follows:

$$H_\lambda(x,y) = \frac{R_\lambda(x,y) - D_\lambda(x,y)}{W_\lambda(x,y) - D_\lambda(x,y)} \quad (1)$$

$H_\lambda(x,y)$ is the calculated reflectance for the pixel (x,y) for the wavelength λ. $R_\lambda(x,y)$ is the measured radiance of the sample for the pixel (x,y) for the wavelength λ. $W_\lambda(x,y)$ is the measured radiance of the calibration tile for the pixel (x,y) for the wavelength λ. $D_\lambda(x,y)$ is the measured radiance of the dark for the pixel (x,y) for the wavelength λ; this was obtained by covering the lens with the cap, which provided the background signal of the camera system (camera + lens).

Following digestion for different periods, two sample slices were cut from the centre of the milk clot cylinder and were placed in a petri dish, as described above. They were scanned using the hyperspectral system (Fig. 1). Then, one sample slice was used for moisture analysis and the other slice was used for acidity analysis, as described below.

2.5. Physicochemical analyses

To determine the mass loss from the milk clot cylinders during digestion, they were weighed before and immediately after static digestion for defined periods (without the protective caps). Mass loss is presented as negative values, as a percentage of the original weight.

The moisture content of a sample slice following HSI analysis was determined by measuring its weight before and after oven drying at 105 °C for 24 h. The moisture content is presented as a percentage of the wet weight before drying.

The sample slice for acidity determination was first weighed. It was then ground with a pestle and mortar and transferred to a clean container. An aliquot of 40 mL of deionized water was used to rinse off the debris from the mortar; this was mixed with the ground sample. The acidity of the sample was determined by titration with 0.01 N NaOH until the pH reached 8.2 and remained stable for 30 s, using a titration device (TitroLine® 7000, SI Analytics, Mainz, Germany). The quantity of NaOH used was recorded and the sample acidity is expressed as milligrams of HCl per gram of sample on a wet basis.

2.6. Hyperspectral data processing

Raw hyperspectral images and spectral data were subjected to data pre-processing and multivariate analysis using R (R Core Team, 2018) and Python. Initially, the background was removed from the hyperspectral images via thresholding and masking. A threshold was calculated using the Otsu thresholding method (Fan & Zhao, 2007; van der Walt et al., 2014) on the hyperspectral image at a wavelength of 1533.68 nm to isolate the samples from their background and from undesirable pixels that exhibited abnormal reflectance values. The image at the wavelength 1533.68 nm was chosen because it had the maximum difference in reflectance values for the background and the sample. After thresholding, a series of morphological operations were performed in different combinations, namely erosion, dilation, opening and small object (pixel/s) removal to obtain the region of interest, i.e. the two sample slices. Next, both sample slices were labelled. The labels were then used to automatically separate each as separate images: one related to moisture analysis and the other related to acidity analysis. Finally, the cleaned and labelled sample images were saved as NumPy arrays for further analysis (Oliphant, 2006). A flowchart of image processing procedures is presented in supplementary Fig. S1.

2.6.1. Partial least squares regression (PLSR)

PLSR is a multivariate regression method that correlates spectral information with predictors (e.g. moisture). It has been used extensively in spectroscopy to deal with the high level of collinearity among variables in the spectral data by projecting the spectra into a latent space that maximizes the description of information related to the predictor. The spectra for each sample are averaged for modelling. An average spectrum per sample is utilized. In this case, a sample was a cylindrical disk of digested milk clot sample. Two datasets (86 spectra each) were obtained, one for moisture analysis and the other for acidity analysis. A range of pre-processing methods was used on the spectra, including standard normal variate (SNV) transformation + Savitzky-Golay smoothing, and first and second order derivatives to minimize noise and enhance the signal-to-noise ratio. The pre-processed datasets were split into calibration sets and validation sets before modelling using PLSR. The split between the calibration and validation datasets was carried out to ensure that samples in both the calibration sets (≈ 70%) and the validation sets (≈ 30%) were representative of the whole dataset. Also, it ensured that samples subjected to the four treatments (two milk types and the presence/absence of pepsin) and the six time points were distributed evenly in both the calibration sets and the validation sets. The calibration datasets were used to develop the calibration models for predicting moisture and acidity respectively. The method of k-fold (number of folds = 5) cross-validation was utilized while developing the calibration models to avoid either over- or under-fitting of the models (Rodriguez, Perez, & Lozano, 2010). The best PLSR models were selected based on the minimum values of both the standard error of calibration (SE_c) and the standard error of cross-validation (SE_{cv}). The corresponding values of the coefficients of determination in calibration (R_c^2) and cross-validation (R_{cv}^2) were maximum for the best-fit models. The models were validated to ensure that they will work efficiently in the future for similar data. For evaluating the prediction accuracy of the developed calibration models, the validation dataset prepared for each dataset was tested with its respective calibration models. Statistical indices, such as the standard error of prediction (SE_p), corresponding coefficients of determination in prediction, slope, intercept, bias and the residual predictive deviation (RPD), were calculated and defined the prediction performance of the PLSR models.

Variable importance in projection (VIP) scores represent the importance of individual × variables (wavelengths) in the PLSR model. It is a useful measure for identifying the variables (wavelengths) that contribute significantly to the y (physicochemical data) variance explanation. VIP scores were calculated and plotted for the best-fit moisture model. The software package “mdatools” in R was used for modelling (Kucheryavskiy, 2020).

2.6.2. Superpixel prediction maps of moisture

To visualize the spatiotemporal distribution of moisture in the samples, selected hyperspectral images for moisture samples were superpixeled; that is, each hyperspectral image was segmented into 25 as well as 500 segments while using superpixel segmentation (Achanta et al., 2012). Each segment (a superpixel) is formed of pixels with higher similarity within a neighbourhood and taking the average spectrum of the pixels in this segment helps to reduce the impact of unwanted pixel-to-pixel variation due to heterogeneous sample surface. The spectra for each segment (a set of individual image pixels) were then averaged to produce a single spectrum per segment. Each of these spectra was fed into the moisture model and a moisture content value was predicted for each segment. The prediction for each segment was then used to create a prediction map for each sample.

2.6.3. Quantile analysis of predicted moisture data and visualization

To better understand the moisture distribution in a sample, all pixels within the pixel-wise moisture map of a sample slice (>3000 pixels) were separated into five equal quantiles based on their predicted moisture values. The use of quantile analysis helps to identify key regions relate to attribute distribution in the sample as well as to reduce the impact of unwanted pixel-to-pixel variation due to heterogeneous sample surface. Each quantile consisted of 20% of the pixels in a sample

image and is referred to as Q1, Q2, Q3, Q4 and Q5, in increasing order of moisture content. The maximum moisture (M_{max}) values of Q1–Q4, which separated the five quantiles, were analysed for their respective changes during digestion. Representative moisture maps displaying only pixels in selected quantiles were produced to demonstrate the distribution of high and low moisture areas in the sample.

2.7. Statistical analysis

Statistical analysis of the physicochemical data and the predicted moisture data was conducted using Minitab version 19.1.1. Significant differences between milk types, presence/absence of pepsin and digestion time points were determined using two-sample t-tests and one-way analysis of variance (ANOVA) with the Fisher's least significant difference (LSD) test. Three-way ANOVA was used to determine significant effects when considering all three variables (milk type, pepsin and digestion time). Significant correlations between mass loss, acidity and moisture were also determined.

3. Results and discussion

3.1. Physicochemical analyses

3.1.1. Change in moisture content during digestion

The moisture contents of the samples at different stages of the static incubation in SGF are presented in Fig. 2. The initial moisture content of the milk clots before incubation was on average 66% (*wt/wt*), with no significant difference between SM and CaSM. When all samples were considered, three-way ANOVA indicated that the moisture contents of the milk clots decreased significantly with the digestion time ($p < 0.001$); it was more pronounced in the presence of pepsin ($p = 0.001$). Despite a trend of higher moisture in the CaSM samples, the effect of milk type was insignificant ($p = 0.06$). For both SM and CaSM, the moisture contents of the samples decreased significantly over time only in the presence of pepsin [Fig. 2(A), $p < 0.05$] and not in the absence of pepsin [Fig. 2(B), $p > 0.2$]. The moisture reduction over time was more pronounced for SM ($p < 0.001$) than for CaSM ($p = 0.04$) [Fig. 2(A)].

These results displayed the unique water expulsion behaviour of the milk clots formed dynamically during gastric digestion; this behaviour contrasted with that of most solid food structures, which take up moisture from the gastric environment during digestion (Mennah-Govela & Bornhorst, 2016a; van der Sman et al., 2020). In agreement with the present study, previous studies have reported that milk clots lose moisture during the first 2–4 h of dynamic in vitro gastric digestion (Li et al., 2022a; Roy et al., 2021; Ye et al., 2019). These observations indicated that endogenous driving forces expel water from the milk clot structures during gastric digestion. As proposed previously, milk clots can undergo structural compaction during gastric digestion, similar to the microsyneresis of cheese curds that expels whey (Barbé et al., 2014; Li et al., 2022a; Qazi, Ye, Acevedo-Fani, & Singh, 2021). The significant effect of pepsin on curd moisture content suggested that protein hydrolysis contributed to the structural compaction of and the moisture removal from the clots (Fig. 2). This may have arisen from the ongoing hydrolysis of the remaining κ-casein, the removal of hydrophilic peptides and the incorporation of hydrophobic peptides into the clot structures.

3.1.2. Acid uptake and mass loss

In contrast to the trend in the moisture content, the acidity increased significantly during the incubation [Fig. 3(A) and 3(B)]. In addition, the overall acidity levels of the clots were significantly higher for SM than for CaSM, ($p < 0.001$) and when incubated without pepsin ($p < 0.001$). After 220 min of incubation, the acidity of the samples ranged from 2.2 mg HCl/g (CaSM with pepsin) to 3.3 mg HCl/g (SM without pepsin). The mass loss from the milk clot cylinders occurred gradually during the static incubation, both with and without pepsin [Fig. 3(C) and 3(D)]. It was significantly greater in the presence of pepsin and at a longer incubation time ($p < 0.05$). There was no significant effect of milk type ($p > 0.1$).

Overall, the skim milk clots took up acid and lost mass significantly during incubation under simulated gastric conditions, irrespective of the presence of pepsin or the type of milk. Acidity expectedly increased during incubation presumably because of the low pH of the SGF, which provides a concentration gradient and a driving force for hydrogen ions to migrate into the clots. The lower acidity of the CaSM clots compared with the SM clots probably arose from the higher calcium and protein contents of the CaSM, which contributed to a higher buffering capacity. The lower acidity of the samples incubated with pepsin was also expected because the cleavage of peptide bonds during protein digestion produces carboxyl and amino groups, which contribute to the buffering capacity in the acidic gastric environment (Luo, Zhan, Boom, & Janssen, 2018). Mass loss from the clots probably occurred because of physical disintegration (e.g. shaking) and chemical processes (e.g. electrostatic repulsion) during incubation in the SGF. During these processes, the buffering capacity appeared to have limited impact, because of the insignificant effect of milk type on mass loss. The presence of pepsin expectedly promoted mass loss, by digesting the proteins and releasing the protein/peptides from the clot.

3.1.3. Interrelationships between parameters

When all samples were considered, the moisture content had a significant negative correlation with acidity ($p < 0.001$). However, for

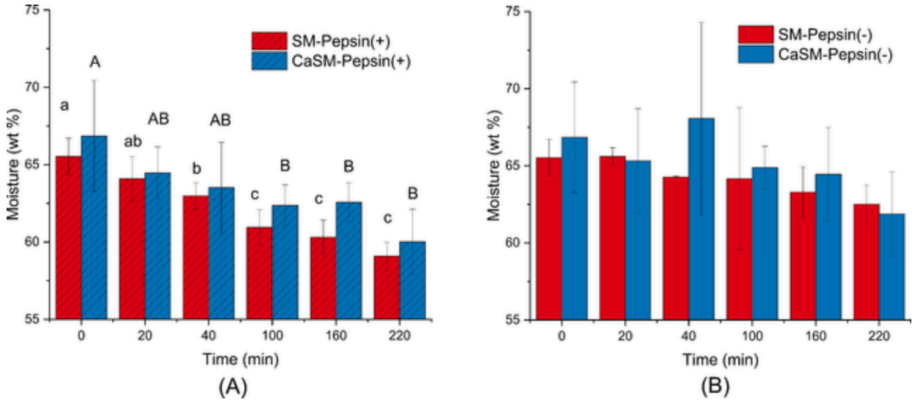

Fig. 2. Moisture contents of milk clots during static incubation in simulated gastric fluid with pepsin (A) and without pepsin (B). SM, skim milk; CaSM, calcium-enriched skim milk. The plus and minus symbols indicate the presence and absence of pepsin in the simulated gastric fluid. Different letters indicate significant differences at different incubation times for SM (lowercase) and CaSM (uppercase) determined using one-way analysis of variance with the Fisher's LSD test.

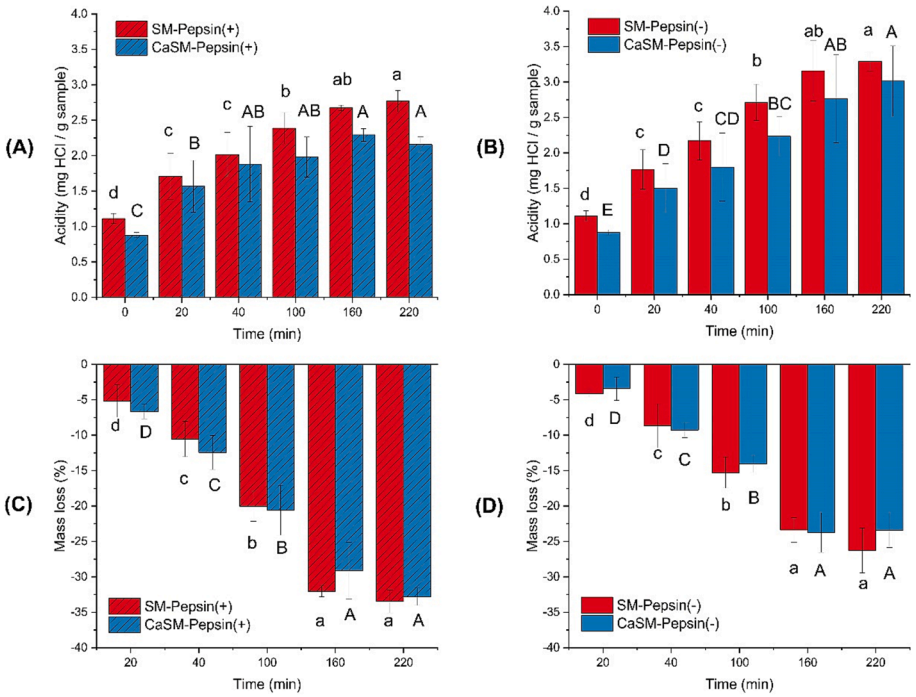

Fig. 3. Acidity (A, B) and mass loss (C, D) of milk clots during static incubation in simulated gastric fluid with pepsin (A, C) and without pepsin (B, D). SM, skim milk; CaSM, calcium-enriched skim milk. The plus and minus symbols indicate the presence and absence of pepsin in the simulated gastric fluid. Different letters indicate significant differences at different incubation times for SM (lowercase) and CaSM (uppercase) determined using one-way analysis of variance with the Fisher's LSD test.

individual combinations of milk type and the presence/absence of pepsin, the negative correlation between moisture content and acidity was significant only when the sample was incubated with pepsin, and it was more significant for SM ($p < 0.001$) than for CaSM ($p = 0.03$). Thus, we demonstrated that the milk clots expelled water while taking up acid during gastric digestion. The contrasting trends suggested that the two processes had very different driving forces, unlike the common behaviour of water convection and diffusion with gastric acid. Similar to the moisture/acidity correlations, greater mass loss was significantly correlated with lower moisture content only when the milk clots were incubated with pepsin (for SM, $p < 0.001$; for CaSM, $p < 0.01$). The expulsion of water expectedly contributed to the loss of wet mass over time. In addition, as the disintegration and the protein hydrolysis would have taken place mostly at the surface, they may have either increased or decreased the moisture content of the remaining clot cylinder, depending on the distribution of moisture within the clot. That is, if the surface of the clot contained more moisture than the centre, surface disintegration would have contributed to reducing the moisture content of the remaining clot cylinder over time, as demonstrated in Fig. 2. To explore this, we mapped the spatiotemporal distribution of moisture within the clot slice used for moisture analysis using prediction models developed based on HSI spectra.

3.2. Performance of prediction models

While we have successfully predicted acidity utilizing hyperspectral imaging previously (Somaratne et al. 2019), in this study, the performance of the acidity model was poor. We tested multiple types of pre-processing as well as other models such as support vector machine, but performance did not improve. A potential reason for this could be the narrow range of values found for acidity that limited our ability to develop the model for acidity. Thus, results of the acidity model are not further discussed.

The pre-processed average spectra for moisture modelling at different time points are presented in Supplementary Fig S2, where the most significant visual difference is observed at 1450 nm and 1200 nm spectral ranges. Table 1 presents the performance summary of the developed PLSR models of moisture, together with the coefficients of determination and standard errors of calibration (SE_c, R_c^2) and cross-validation (SE_{cv}, R_{cv}^2) and with the number of latent variables (LVs) used. Statistical indices such as the coefficients of determination and standard errors of prediction (SE_p, R_p^2) and the calculated bias for the validation set are also presented. The SNV transformed + smoothed data showed the best fit for the moisture model, yielding an R_{cv}^2 of 0.75 and an SE_{cv} of 1.46. The first derivative transformed data also showed good results, yielding an R_{cv}^2 of 0.73 and an SE_{cv} of 1.52. The raw and second derivative transformed data showed rather poor performance, yielding

Table 1
Performance summary of the developed partial least squares regression models.

Pre-processing	Calibration							Validation						
	n_c	LV	R_c^2	SE_c	R_{cv}^2	SE_{cv}	Bias	n_v	R_p^2	SE_p	Slope	Bias	RPD	Intercept
Raw	60	4	0.53	1.99	0.42	2.28	–0.06	26	0.36	2.61	0.35	1.16	1.28	0.01
SNV + smoothing	60	6	0.85	1.11	0.75	1.46	–0.04	26	0.69	1.82	0.70	0.39	1.84	0.73
First derivative	60	4	0.83	1.19	0.73	1.52	0.06	26	0.66	1.90	0.66	0.75	1.76	0.95
Second derivative	60	2	0.69	1.61	0.49	2.08	0.00	26	0.54	2.23	0.53	0.75	1.50	–0.26

SNV, standard normal variate; LV, number of latent variables; R_c^2, coefficient of determination of calibration; SE_c, standard error of calibration; R_{cv}^2, coefficient of determination of cross-validation; SE_{cv}, standard error of cross-validation; R_p^2, coefficient of determination of prediction; SE_p, standard error of prediction; RPD, residual predictive deviation.

R^2_{cv} values of 0.42 and 0.49 and SE_{cv} values of 2.28 and 2.08 respectively.

The models were also validated using their corresponding independent validation sets. It should be noted that the samples in the validation set were not included in the development of the calibration model. The SNV transformed and smoothed model with six latent variables showed the best predictions for the validation dataset, as indicated by an R^2_p of 0.69, an SE_p of 1.82 and a bias of 0.39. Also, the slope was 0.70 with a low intercept of 0.73. The first derivative model also showed similar performance. As the SNV transformed + smoothed data showed the best performance, it was further used to produce moisture prediction maps.

The VIP scores show that the PLSR model was mainly affected by changes in water content, structural changes and changes in proteins (see Supplementary Fig. S3 and assignment of important variables).

3.3. Spatiotemporal mapping of moisture distribution

3.3.1. Superpixel prediction maps

Fig. 4 shows the superpixel prediction maps (25 and 500 superpixels) of moisture at different stages during the static incubation of the skim milk clots in SGF, with and without pepsin. As can be seen from both 25-superpixel and 500-superpixel prediction maps, all samples generally displayed trends of decreasing moisture during prolonged incubation in SGF; this was most pronounced visually for SM in the presence of pepsin, agreeing with the bulk moisture results presented in Fig. 2. Interestingly, the distribution of moisture within each sample slice indicated that moisture was generally higher in the central area and lower near the surface (Fig. 4). This occurred for all samples, regardless of milk type or the presence/absence of pepsin.

3.3.2. Distribution of high and low moisture zones

To better illustrate the moisture distribution within a sample, we divided all the pixels in a prediction map into five equal quantiles based on their predicted moisture content. Each quantile consisted of 20% of all pixels in a prediction map. Fig. 5(A) presents the moisture maps of the same samples as in Fig. 4, but only the pixels in the lowest moisture quantile (Q1, lowest 20%) and those in the highest moisture quantile (Q5, highest 20%). These moisture maps clearly show that the majority of the highest-moisture pixels (purple to dark blue) were mostly centralized in each sample. In contrast, the pixels in the lowest-moisture quantile (light blue to green) were located around the surface, which was in contact with the surrounding SGF during digestion.

Most solid food structures have a decreasing moisture gradient from the surface to the centre during gastric digestion as the gastric juice diffuses into the food. This finding further displayed the unique movement of moisture in the milk clots that form in the stomach. It also disproves the speculation raised earlier that, if the moisture was higher at the clot surface, the mass loss from the surface would contribute to the observed moisture reduction over time. As the opposite was found, i.e. the clot surface was lower in moisture (Figs. 4 and 5), the disintegration and dissociation of the clots at the surface should have increased the moisture content of the remaining clot. Despite this, the moisture content still decreased over time, further highlighting a strong driving force for moisture expulsion. This is discussed below.

Furthermore, it appeared that, during digestion, the moisture contents of the lowest moisture zones close to the clot surface did not change as much as those of the highest moisture zones [Fig. 5(A)]. This is further demonstrated by the SM with pepsin samples in Fig. 5(B), which had the most pronounced moisture decrease over time [Fig. 2(A)]. In Fig. 5(B), the pixels in Q1 and Q5 (lowest and highest moisture) are presented in the top row and the pixels in Q3 and Q4 (mid-high moisture; 40–80th percentile) are presented in the bottom row. Consistent with the observation that the highest moisture zones were centralized and the lowest moisture zones were located at the surface, the pixels in Q3 and Q4 were located mostly in the in-between area in the sample slice. In addition, Q3, Q4 and Q5 had greater changes in colour during digestion (from purple/dark blue to light blue), indicating their greater moisture reductions than that of the lowest moisture zone Q1 over time. This was supported by statistical analysis of the maximum moisture (M_{max}) values of Q1, Q2, Q3 and Q4 (which separated Q1–Q5). During the 220 min of static incubation, the M_{max} of Q1 first decreased significantly from 0 to 100 min and then from 100 to 220 min, whereas the M_{max} of Q2, Q3 and Q4 had three significant decreases, from 0 to 40 min, from 40 to 100 min and from 100 to 220 min ($p < 0.05$, one-way ANOVA with Fisher's LSD test). In addition, consistent across all samples (milk types and presence/absence of pepsin), the M_{max} of Q1 had the smallest decrease among the different quantiles over time. From 0 to 220 min, the M_{max} values of Q2–Q4 decreased, on average, 25% more than the M_{max} value of Q1. There were slight differences among Q2, Q3 and Q4, with a trend of the higher moisture quantiles having greater moisture loss over time.

In summary, the quantile analysis results demonstrated that the moisture loss from the milk clots in the gastric environment was slower in the lowest moisture zones located at the clot surfaces, which were in direct contact with the SGF, and was faster in the medium to high moisture zones located closer to the centre. It appeared that moisture diffusion driven by the concentration gradient was not a crucial factor in determining the movement of moisture within gastric milk clots. This applied to both bulk moisture transfer between the clot and the surrounding aqueous environment (Fig. 2) and the moisture transfer within the clot (Fig. 5). Instead, bulk water movement caused by the dynamic restructuring of the clots appeared to be the dominating mechanism. Unlike other previously investigated food structures, such as protein gels (Deng et al., 2020; Somaratne et al., 2019), the gastric milk clot is unique in that it forms and continuously evolves under a dynamic process involving a combination of enzymatic, physical and chemical processes (Huppertz & Chia, 2020; Li et al., 2021; Ye et al., 2019). As a result, the structure of milk clots is more heterogeneous and open, and is more susceptible to further structural evolvement. It could also explain the larger mass loss from the clot during incubation in the present study than previously reported for whey protein gels (Deng et al., 2020). With respect to moisture, instead of closely bonding to the proteins, as in protein gels, a considerable proportion of the water is probably trapped or loosely held by the protein matrix in the milk clot. Large gaps and water channels are probably present in the dynamically formed milk clot structures, allowing greater bulk water movement from the clot to the surrounding environment.

3.4. Discussion of physicochemical changes and possible mechanisms

Based on the findings of this study, we propose that the driving force for moisture expulsion from milk clots during gastric digestion is the structural compaction of the clot over time, which takes place mainly at the surface, caused by both proteolysis and acidification.

3.4.1. Effect of pepsin hydrolysis

The compaction of milk clot structures during digestion expels water and results in a loss of moisture. This process is similar to the syneresis of cheese curds, resulting from the increased binding affinity among the proteins that promotes the gradual fusion of the protein network (Barbé et al., 2014; Li et al., 2022a; Qazi et al., 2021; Renkema, 2004). The preferential hydrolysis of κ-caseins by pepsin during early digestion (when the pH is around 6.0) removes the more hydrophilic and negatively charged caseinomacropeptides, promoting aggregation and further fusion of the remaining caseins and the hydrophobic para-κ-casein. During the later stages of digestion, other hydrophobic peptides resulting from proteolysis also probably associate with the clots whereas the more hydrophilic peptides are more readily emptied from the stomach, as illustrated by the different peptide bands in sodium dodecyl sulphate polyacrylamide gel electrophoresis gels between the clots and the emptied digesta in previous studies (Li et al., 2022b; Roy et al., 2021). We propose that, in the present study, proteolysis by pepsin contributed to the structural compaction at the clot surface by altering

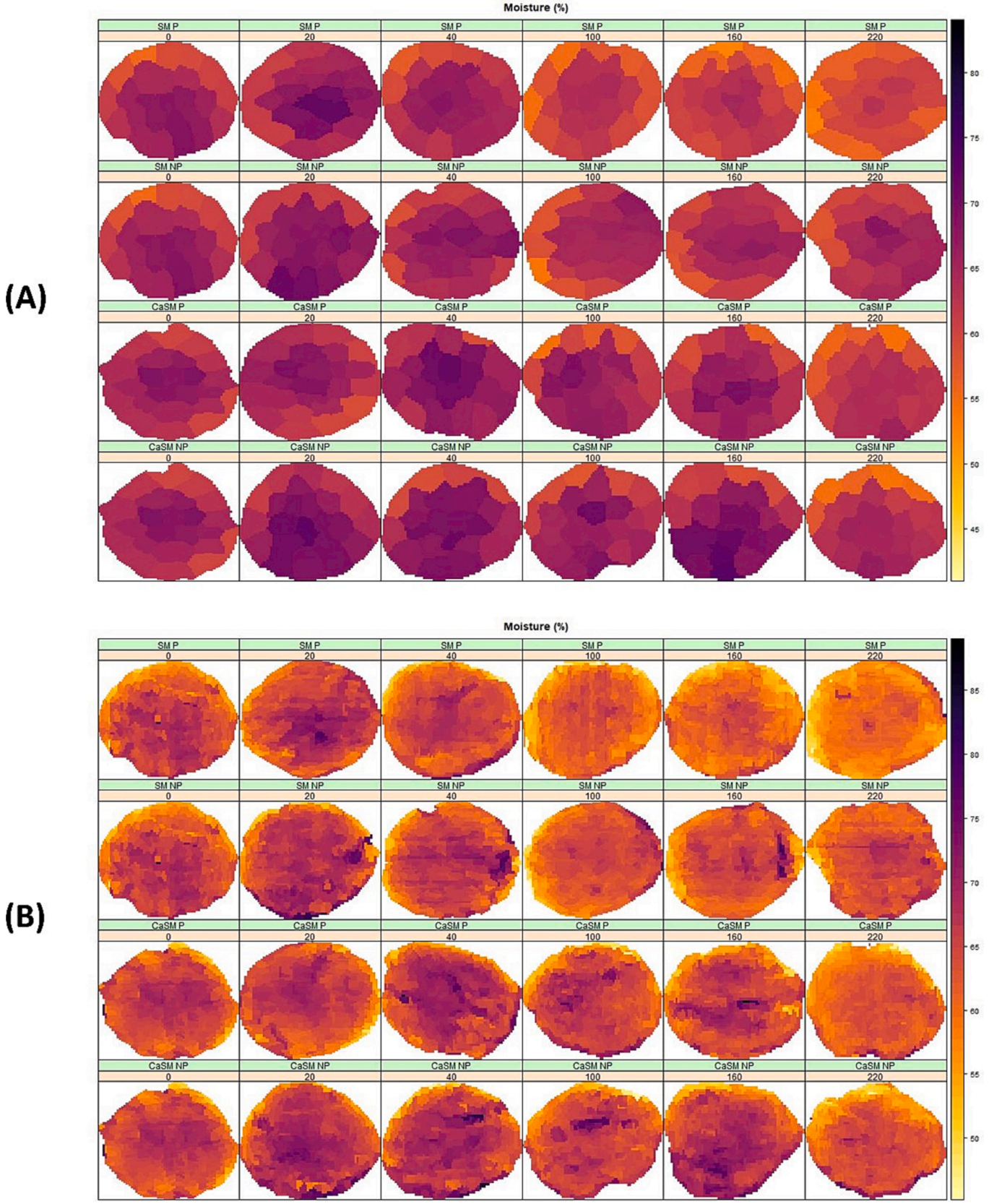

Fig. 4. Representative superpixel moisture prediction maps of milk clots during static incubation in simulated gastric juice (0–220 min): 25 superpixels (A) and 500 superpixels (B). SM, skim milk; CaSM, calcium-enriched skim milk; P, incubation with pepsin; NP, incubation without pepsin.

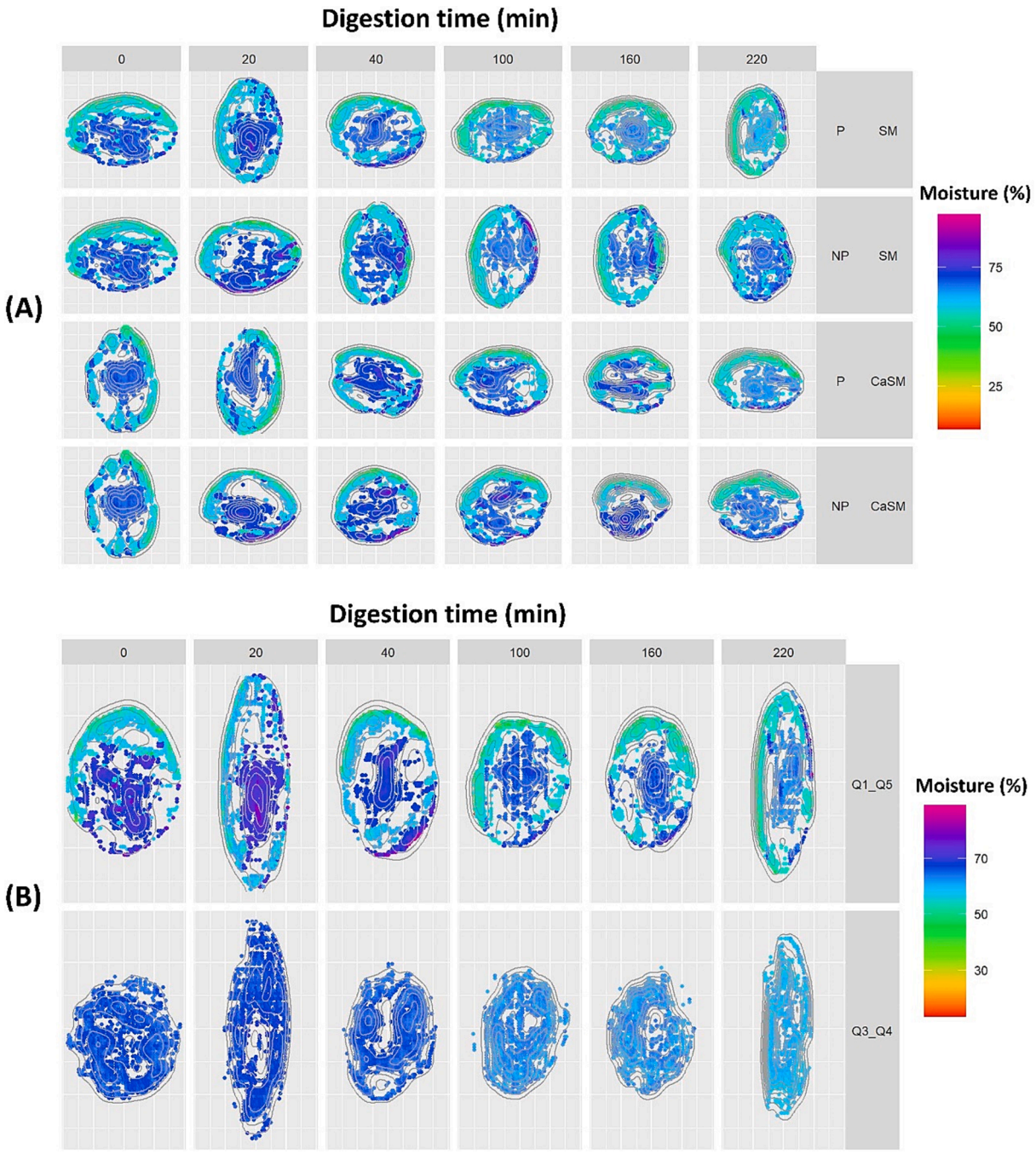

Fig. 5. (A) Moisture prediction maps plotting the pixels in both Q1 (lowest moisture group) and Q5 (highest moisture group) of representative samples. SM, skim milk; CaSM, calcium-enriched skim milk; P, incubation with pepsin; NP, incubation without pepsin; (B) Moisture prediction maps of a representative SM sample digested with pepsin. Maps in the top row display pixels in Q1 and Q5. Maps in the bottom row display pixels in Q3 and Q4 (predicted moisture in the 40–80th percentile).

the composition of the proteins and peptides. This could explain why the lowest moisture zones were present at the surface (Fig. 5).

3.4.2. *Effect of acidification*

In addition to the effect of pepsin, the structural changes in the milk clots may have also been caused by a chemical process, i.e. pH-modulated changes in protein charge and calcium dissolution. The milk clots used for the static incubation formed when the surrounding gastric liquid phase had a fairly high pH of around 6.0. The internal pH of the clots was probably even higher because of the buffering capacity of the milk components and limited access to the more acidic aqueous environment, as demonstrated previously (Roy et al., 2022). At this pH level, milk proteins are still negatively charged and the CCP remains largely intact in the casein micelles. It has been reported that the dissolution of milk calcium had barely started at 20 min of dynamic gastric digestion under similar conditions (Choki et al., 2021). During the static incubation, acid transfer into the clots (Fig. 3) would have gradually altered the charges on the proteins and solubilized the CCP. As the pH decreased, charge neutralization from pH ≈ 6 to pH ≈ 4.6 would have reduced the electrostatic repulsive forces between proteins in the clot matrix and would have contributed to their greater binding affinity and compaction. Further pH reduction below the isoelectric point, which presumably occurs first at the surface, may have led to swelling because of the increasing positive charges on the proteins, which

promotes digestion by increasing the influx of acid and pepsin (van der Sman et al., 2020). In the present study, this swelling effect was not apparent, as demonstrated by the decreasing moisture content of the clots, including the clot surface (Figs. 2 and 5). However, it may have contributed to the surface disintegration and mass loss [Fig. 3(C) and 3 (D)]. A complex interplay and counterbalance between structural compaction and water expulsion from the interior and the local swelling and disintegration at the surface may have resulted in the slower moisture reduction over time of the low moisture zones at the surface than of the higher-moisture zones in the centre [Fig. 5(B)]. The interior of the clots would have had fewer complex physicochemical changes, mainly as a result of the surface compaction process that drove water expulsion via internal gaps and water channels.

Another consequence of acid transfer to the clot is the dissolution of the CCP in the casein micelles. CCP contributes to the clot structure; its dissolution during dynamic gastric digestion would alter the maintaining forces within the protein network and influence its structural development (Huppertz & Lambers, 2020; Li et al., 2022a). During acid- and acid–rennet-induced gelation, which mechanistically resembles the pepsin/acid-modulated gastric coagulation of milk, CCP dissolution within the gel network as the pH decreases induces a restructuring process that leads to a coarser network with straighter strands that contribute to greater permeability and rigidity of the gels (Li, Delger, Dave, Singh, & Ye, 2023; Lucey, Tamehana, Singh, & Munro, 2000; Renkema, 2004). In gastric milk clots, this calcium dissolution process might contribute to water expulsion and structural compaction. Higher concentrations of calcium and protein, as in the CaSM, may restrict the extent of structural development and water expulsion during digestion, because of the formation of a more compact and rigid network (Panthi et al., 2019). This could explain the less pronounced moisture loss of the CaSM clots than of the SM clots during the digestion process (Fig. 2).

4. Conclusions

This study demonstrated the effects of milk type (different protein and calcium contents) and pepsin on the movement of moisture and acid during the gastric digestion of skim milk. For the first time, we explored the use of HSI to study the digestion of milk and successfully mapped the spatiotemporal distribution of moisture within the milk clots that form dynamically under gastric digestion conditions. In contrast to acid uptake into the milk clot structures during gastric digestion, moisture within the milk clots decreased significantly over time when digested with pepsin. The spatiotemporal mapping of moisture based on HSI spectra modelling provided novel insights that the surface of the clot in contact with gastric fluids was lower in moisture content than the centre, and that the moisture decreased more rapidly in the centre than at the surface of the clots during digestion, where both pepsin hydrolysis and acidification probably played important roles. This work demonstrated another novel application of HSI in the field of food science research. The unique findings on the movements of moisture and acid during the gastric digestion of milk contribute to a deeper understanding of the gastric coagulation behaviour of milk-based foods that plays a critical role in their digestive dynamics and nutritional outcomes.

CRediT authorship contribution statement

Siqi Li: Conceptualization, Methodology, Investigation, Formal analysis, Visualization, Project administration, Writing – original draft. **Yash Dixit:** Methodology, Software, Formal analysis, Visualization, Writing – original draft. **Marlon M. Reis:** Methodology, Software, Formal analysis, Writing – review & editing. **Harjinder Singh:** Funding acquisition, Writing – review & editing. **Aiqian Ye:** Conceptualization, Funding acquisition, Resources, Writing – review & editing.

Declaration of Competing Interest

The authors declare that they have no known competing financial interests or personal relationships that could have appeared to influence the work reported in this paper.

Data availability

Data will be made available on request.

Acknowledgements

This work was supported by the Ministry of Business, Innovation and Employment (Wellington, New Zealand), via the research programme “New Zealand Milks Mean More”, and the Tertiary Education Commission via the Riddet Institute, a New Zealand Centre of Research Excellence.

The authors acknowledge Kamalam Natarajan (Riddet Institute, Massey University) and Christine Tu (AgResearch) for performing the experiments and Clive Bardell (Massey University) for crafting the tools for sample preparation. We thank Claire Woodhall for proofreading the manuscript.

References

Achanta, R., Shaji, A., Smith, K., Lucchi, A., Fua, P., & Süsstrunk, S. (2012). SLIC superpixels compared to state-of-the-art superpixel methods. *IEEE Transactions on Pattern Analysis and Machine Intelligence, 34*(11), 2274–2282. https://doi.org/10.1109/TPAMI.2012.120

Barbé, F., Ménard, O., Le, Y., Buffière, C., Famelart, M., Laroche, B., Le, S., Rémond, D., & Dupont, D. (2014). Acid and rennet gels exhibit strong differences in the kinetics of milk protein digestion and amino acid bioavailability. *Food Chemistry, 143*, 1–8. https://doi.org/10.1016/j.foodchem.2013.07.100

Bornhorst, G. M., & Singh, R. P. (2014). Gastric digestion in vivo and in vitro: How the structural aspects of food influence the digestion process. *Annual Review of Food Science and Technology, 5*(1), 111–132. https://doi.org/10.1146/annurev-food-030713-092346

Brodkorb, A., Egger, L., Alminger, M., Alvito, P., Assunção, R., Ballance, S., … Recio, I. (2019). INFOGEST static in vitro simulation of gastrointestinal food digestion. *Nature Protocols, 14*(4), 991–1014. https://doi.org/10.1038/s41596-018-0119-1

Choki, K., Li, S., Ye, A., Jameson, G. B., & Singh, H. (2021). Fate of hydroxyapatite nanoparticles during dynamic *in vitro* gastrointestinal digestion: The impact of milk as a matrix. *Food & Function, 12*(6), 2760–2771. https://doi.org/10.1039/d0fo02702b

Deng, R., Mars, M., van der Sman, R. G. M., Smeets, P. A. M., & Janssen, A. E. M. (2020). The importance of swelling for in vitro gastric digestion of whey protein gels. *Food Chemistry, 330*(May), Article 127182. https://doi.org/10.1016/j.foodchem.2020.127182

Fan, J., & Zhao, F. (2007). Two-dimensional Otsu’s curve thresholding segmentation method for gray-level images. *Acta Electronica Sinica, 35*(4), 751.

Guo, Q., Ye, A., Singh, H., & Rousseau, D. (2020). Destructuring and restructuring of foods during gastric digestion. *Comprehensive Reviews in Food Science and Food Safety, 19*(4), 1658–1679. https://doi.org/10.1111/1541-4337.12558

Huppertz, T., & Chia, L. W. (2020). Milk protein coagulation under gastric conditions: A review. *International Dairy Journal, 113*, Article 104882. https://doi.org/10.1016/j.idairyj.2020.104882

Huppertz, T., & Lambers, T. T. (2020). Influence of micellar calcium phosphate on in vitro gastric coagulation and digestion of milk proteins in infant formula model systems. *International Dairy Journal, 107*, Article 104717. https://doi.org/10.1016/j.idairyj.2020.104717

Jiang, X., Hu, X., Huang, H., Tian, J., Bu, Y., Huang, D., & Luo, H. (2021). Detecting total acid content quickly and accurately by combining hyperspectral imaging and an optimized algorithm method. *Journal of Food Process Engineering, 44*(11), e13844.

Kong, F., Oztop, M. H., Singh, R. P., & McCarthy, M. J. (2013). Effect of boiling, roasting and frying on disintegration of peanuts in simulated gastric environment. *LWT – Food Science and Technology, 50*(1), 32–38. https://doi.org/10.1016/j.lwt.2012.07.044

Kucheryavskiy, S. (2020). Mdatools – R package for chemometrics. *Chemometrics and Intelligent Laboratory Systems, 198*, Article 103937. https://doi.org/10.1016/j.chemolab.2020.103937

Li, S., Delger, M., Dave, A., Singh, H., & Ye, A. (2023). Acid and rennet gelation properties of sheep, goat, and cow milks: Effects of processing and seasonal variation. *Journal of Dairy Science*. https://doi.org/10.3168/jds.2022-22561

Li, S., Pan, Z., Ye, A., Cui, J., Dave, A., & Singh, H. (2022a). Structural and rheological properties of the clots formed by ruminant milks during dynamic in vitro gastric digestion: effects of processing and species. *Food Hydrocolloids*, *126*(December 2021), 107465. https://doi.org/10.1016/j.foodhyd.2021.107465.

Li, S., Ye, A., Pan, Z., Cui, J., Dave, A., & Singh, H. (2022b). Dynamic in vitro gastric digestion behavior of goat milk: Effects of homogenization and heat treatments. *Journal of Dairy Science, 105*(2), 965–980. https://doi.org/10.3168/jds.2021-20980

Li, S., Ye, A., & Singh, H. (2021). Impacts of heat-induced changes on milk protein digestibility: A review. *International Dairy Journal, 123*, Article 105160. https://doi.org/10.1016/j.idairyj.2021.105160

Liu, Y., Pu, H., & Sun, D. W. (2017). Hyperspectral imaging technique for evaluating food quality and safety during various processes: A review of recent applications. *Trends in Food Science and Technology, 69*, 25–35. https://doi.org/10.1016/j.tifs.2017.08.013

Lucey, J. A., Tamehana, M., Singh, H., & Munro, P. A. (2000). Rheological properties of milk gels formed by a combination of rennet and glucono-δ-lactone. *Journal of Dairy Research, 67*(3), 415–427. https://doi.org/10.1017/S0022029900004246

Luo, Q., Zhan, W., Boom, R. M., & Janssen, A. E. M. (2018). Interactions between acid and proteins under in vitro gastric condition–a theoretical and experimental quantification. *Food & Function, 9*(10), 5283–5289. https://doi.org/10.1039/c8fo01033a

Mennah-Govela, Y. A., & Bornhorst, G. M. (2016a). Acid and moisture uptake in steamed and boiled sweet potatoes and associated structural changes during in vitro gastric digestion. *Food Research International, 88*(Part B), 247–255. https://doi.org/10.1016/j.foodres.2015.12.012

Mennah-Govela, Y. A., & Bornhorst, G. M. (2016b). Mass transport processes in orange-fleshed sweet potatoes leading to structural changes during in vitro gastric digestion. *Journal of Food Engineering, 191*, 48–57. https://doi.org/10.1016/j.jfoodeng.2016.07.004

Mennah-Govela, Y. A., Swackhamer, C., & Bornhorst, G. M. (2021). Gastric secretion rate and protein concentration impact intragastric pH and protein hydrolysis during dynamic *in vitro* gastric digestion. *Food Hydrocolloids for Health, 1*(May), Article 100027. https://doi.org/10.1016/j.fhfh.2021.100027

Mulet-Cabero, A. I., Torcello-Gómez, A., Saha, S., Mackie, A. R., Wilde, P. J., & Brodkorb, A. (2020). Impact of caseins and whey proteins ratio and lipid content on in vitro digestion and ex vivo absorption. *Food Chemistry, 319*(February), Article 126514. https://doi.org/10.1016/j.foodchem.2020.126514

Nau, F., Le Feunteun, S., Le Gouar, Y., Henry, G., Pasco, M., Guérin-Dubiard, C., Nyemb-Diop, K., & Dupont, D. (2022). Spatial-temporal mapping of the intra-gastric pepsin concentration and proteolysis in pigs fed egg white gels. *Food Chemistry, 389*(January). https://doi.org/10.1016/j.foodchem.2022.133132

Oliphant, T. E. (2006). *Guide to NumPy*. Trelgol Publishing USA.

Panthi, R. R., Kelly, A. L., O'Callaghan, D. J., & Sheehan, J. J. (2019). Measurement of syneretic properties of rennet-induced curds and impact of factors such as concentration of milk: A review. *Trends in Food Science and Technology, 91*(January), 530–540. https://doi.org/10.1016/j.tifs.2019.07.023

Piper, D. W., & Fenton, B. H. (1965). pH stability and activity curves of pepsin with special reference to their clinical importance. *Gut, 6*(5), 506–508. https://doi.org/10.1136/gut.6.5.506

Qazi, H. J., Ye, A., Acevedo-Fani, A., & Singh, H. (2021). In vitro digestion of curcumin-nanoemulsion-enriched dairy protein matrices: Impact of the type of gel structure on the bioaccessibility of curcumin. *Food Hydrocolloids, 117*(February), Article 106692. https://doi.org/10.1016/j.foodhyd.2021.106692

R Core Team. (2018). *R: A language and environment for statistical computing*. R Foundation for Statistical Computing.

Reis, M. M., Dixit, Y., Carr, A., Tu, C., Palevich, F., Gupta, T., & Reis, M. G. (2023). Hyperspectral imaging through vacuum packaging for monitoring cheese biochemical transformation caused by Clostridium metabolism. *Food Research International, 169*, Article 112866. https://doi.org/10.1016/j.foodres.2023.112866

Renkema, J. M. S. (2004). Relations between rheological properties and network structure of soy protein gels. *Food Hydrocolloids, 18*(1), 39–47. https://doi.org/10.1016/S0268-005X(03)00040-7

Rodriguez, J. D., Perez, A., & Lozano, J. A. (2010). Sensitivity analysis of k-fold cross validation in prediction error estimation. *IEEE Transactions on Pattern Analysis and Machine Intelligence, 32*(3), 569–575. https://doi.org/10.1109/TPAMI.2009.187

Roy, D., Moughan, P. J., Ye, A., Hodgkinson, S. M., Stroebinger, N., Li, S., Dave, A. C., Montoya, C. A., & Singh, H. (2022). Structural changes in milk from different species during gastric digestion in piglets. *Journal of Dairy Science, 105*(5), 3810–3831. https://doi.org/10.3168/jds.2021-21388

Roy, D., Ye, A., Moughan, P. J., & Singh, H. (2021). Structural changes in cow, goat, and sheep skim milk during dynamic in vitro gastric digestion. *Journal of Dairy Science, 104*(2), 1394–1411. https://doi.org/10.3168/jds.2020-18779

Somaratne, G., Reis, M. M., Ferrua, M. J., Ye, A., Nau, F., Floury, J., Dupont, D., Singh, R. P., & Singh, J. (2019). Mapping the spatiotemporal distribution of acid and moisture in food structures during gastric juice diffusion using hyperspectral imaging. *Journal of Agricultural and Food Chemistry, 67*(33), 9399–9410. https://doi.org/10.1021/acs.jafc.9b02430

van der Sman, R. G. M., Houlder, S., Cornet, S., & Janssen, A. (2020). Physical chemistry of gastric digestion of proteins gels. *Current Research in Food Science, 2*, 45–60. https://doi.org/10.1016/j.crfs.2019.11.003

van der Walt, S., Schönberger, J. L., Nunez-Iglesias, J., Boulogne, F., Warner, J. D., Yager, N., Gouillart, E., & Yu, T. (2014). scikit-image: Image processing in Python. *PeerJ, 2*, e453.

Yang, M., Ye, A., Yang, Z., Everett, D. W., Gilbert, E. P., & Singh, H. (2022). Kinetics of pepsin-induced hydrolysis and the coagulation of milk proteins. *Journal of Dairy Science, 105*(2), 990–1003. https://doi.org/10.3168/jds.2021-21177

Ye, A., Cui, J., Dalgleish, D., & Singh, H. (2016). Formation of a structured clot during the gastric digestion of milk: Impact on the rate of protein hydrolysis. *Food Hydrocolloids, 52*, 478–486. https://doi.org/10.1016/j.foodhyd.2015.07.023

Ye, A., Liu, W., Cui, J., Kong, X., Roy, D., Kong, Y., Han, J., & Singh, H. (2019). Coagulation behaviour of milk under gastric digestion: Effect of pasteurization and ultra-high temperature treatment. *Food Chemistry, 286*, 216–225. https://doi.org/10.1016/j.foodchem.2019.02.010

Zhu, Y., Zou, X., Shen, T., Shi, J., Zhao, J., Holmes, M., & Li, G. (2016). Determination of total acid content and moisture content during solid-state fermentation processes using hyperspectral imaging. *Journal of Food Engineering, 174*, 75–84. https://doi.org/10.1016/j.jfoodeng.2015.11.019